Model for longitudinal-optical phonons and electron-phonon coupling in GaAs-$Ga_{1-x}Al_xAs$ multilayer structures

C. Guillemot and F. Clérot
Centre National d'Etudes des Télécommunications, 22301 Lannion CEDEX, France
(Received 28 January 1991)

A continuum theory is developed to investigate the properties of the long-wavelength longitudinal-optical phonons in GaAs-$Ga_{1-x}Al_xAs$ multilayer structures and the associated electron-phonon interaction. Depending on the layer, the relative ionic displacements are related to GaAs or GaAs-type longitudinal-optical phonons and treated in the framework of the Born-Huang model, generalized to include isotropic dispersion effects in the Brillouin-zone center. For double heterostructures, a finite number of quantized confined modes is found. The interplay between the long-range Coulomb interaction, which couples the vibrations of adjacent GaAs layers, and confinement effects, which prevent the displacements of adjacent GaAs layers to overlap, is elucidated in the case of superlattices. The strength of the electron-phonon coupling in double heterostructures is reduced as compared with the electron–bulk-phonon effective coupling strength for quantum-well widths smaller than 100 Å.

I. INTRODUCTION

Optical phonons in GaAs/AlAs superlattices have been studied by an increasing number of authors in the last few years, both experimentally and theoretically. On the experimental side, Brillouin-zone-center phonons have been investigated for a superlattice wave vector perpendicular to the plane of the layers by Raman scattering experiments in the backscattering configuration.[1–6] The measured energies of the longitudinal-optical (LO) modes confined in the GaAs layer lie on the bulk LO-phonon dispersion curve, provided that the relevant wave vector is the confinement wave vector given by $k=n\pi/[(m+x)a]$; here m is the number of monolayers of the GaAs layer, n refers to the order of the confined mode, and x lies between 0.5 and 1.[5,7–9] Therefore the superlattice normal modes are well accounted for by confined phonons for superlattice wave vectors perpendicular to the layers. Raman scattering experiments have been performed in the right-angle configuration[10] where the in-plane component of the phonon wave vector is nonzero. Although the layer widths were too large for a shift of phonon frequencies to occur, the usual bulk selection rules for longitudinal- and transverse-optical (TO) modes were found to be inverted, revealing again that the confinement wave vector was the physically meaningful wave vector.

From the theoretical point of view, approaches of different complexity have been proposed. Microscopic theories aim at solving the equations of motion for atomic displacements by diagonalizing the standard dynamical matrix. Several authors have calculated phonon modes in superlattices within a linear-chain model.[11–13] This model can only describe modes propagating along the superlattice axis; the agreement with experiments is fairly good. More recently, the shell model[14] and the rigid-ion model[15,16] were used to calculate GaAs/AlAs superlattice phonons propagating in an arbitrary direction. The long-range Coulomb force, which appears whenever the atomic displacements have a longitudinal character, causes a large anisotropy in the dispersion curve of the superlattice optical modes: the frequencies of the long-wavelength modes approach differential limits depending on the directions of propagation relative to the axis of the superlattice. This anisotropy is well marked for the $n=1$ LO and TO confined modes because the total dipole moment within the considered layer is large. On the contrary, the net dipole moment in each layer is small for higher-order modes because of the fast oscillation of the phonon envelope wave function or because of their symmetry. Therefore they do not show a strong angular dispersion in their long-wavelength frequency curve except by mixing with the $n=1$ modes. In accordance with the above-mentioned theories, Huang and Zhu[17,18] have accounted for the anisotropy of the superlattice normal modes in the Brillouin-zone center, within a microscopic model where the atomic displacements are simulated by a superlattice of dipoles.

Beside these microscopic approaches, a number of macroscopic models have been developed to calculate the envelope function of the atomic displacements. Macroscopic models are attractive not only due to their simplicity but also because they allow the calculation of the Fröhlich-type electron-phonon interaction since they directly provide the polarization field due to optical phonons as a continuous function of spatial coordinates. The Fröhlich electron-phonon interaction is of considerable interest because it governs the electronic behavior in many situations such as high field transport or electron trapping in a quantum well. The dielectric continuum model has been widely used in heterostructures and slabs.[19–21] However, it is now well recognized[17,22] that the dielectric continuum model cannot lead to unambiguous solutions for the phonon modes: owing to the neglect of the dispersion in the bulk-phonon frequencies, all LO confined modes are completely degenerate and any of

their linear combinations can be taken as normal modes of the system. Besides, the interface modes, although rigorously derived from the Maxwell relations in the dielectric continuum model, cannot hybridize with the confined modes and present displacements exponentially decreasing from the interfaces: this behavior is not reproduced by microscopic theories for long-wavelength phonons. In an attempt to generalize the dielectric continuum model so as to take into account effects of the dispersion of the bulk mode frequencies, Babiker[23] proposed an isotropic model for dispersive LO phonons. However, he used hydrodynamic boundary conditions at interfaces which are unsuitable for optical phonons and are not consistent with the equations of motion used inside each layer. Consequently, the calculated normal modes are not orthogonalized to each other. Boundary conditions for the envelope function of the normal modes have been investigated by Akera and Ando on a microscopic basis for various semiconductor heterostructures.[24] In GaAs-AlAs heterostructures, where the GaAs and AlAs bulk optical bands have a large gap between them, the boundary condition that the envelopes should vanish at interfaces is shown to be applicable whatever the wave-vector direction is. As this is the condition used in the dielectric continuum model for confined modes, the electron-phonon interaction has been calculated within this continuum model.[25] Finally, in an attempt to establish an equivalent of the Fröhlich interaction in superlattices from their microscopic model, Huang and Zhu conclude that the potentials of the normal modes cannot be described by simple analytical expressions because the frequency dispersion has the effect of mixing the dielectric interface modes with the bulklike confined modes.[17]

Although the frequency spectra and the atomic displacements of the optical phonons are now well studied for GaAs/AlAs superlattices, a reliable and simple approach seems still to be lacking for the Fröhlich interaction in heterostructures. Moreover, most of the theoretical work has been devoted to the AlAs/GaAs system whereas most of the experimental studies on the polar interaction between electrons and optical phonons have been performed on GaAs-$Ga_{1-x}Al_xAs$ heterostructures.[26–29] In the case of GaAs-AlAs heterostructures, the GaAs bulk optical bands do not overlap at all with the AlAs bulk optical bands. Consequently, GaAs/AlAs superlattice phonon modes result from a hybridization of the semiconductor (GaAs or AlAs) LO and TO bulk modes. On the contrary, III-V mixed crystals such as $Ga_{1-x}Al_xAs$ are known to exhibit an optical-phonon two-mode behavior with two zone-center LO frequencies (similar results hold for TO modes) which lie somewhat between the pure GaAs LO and TO zone-center ones for the GaAs-like modes and between the pure AlAs LO and TO zone-center ones for the AlAs-like modes (Fig. 1).

The purpose of this paper is the formulation of a continuum theory for the polar optical modes in GaAs-$Ga_{1-x}Al_xAs$ heterostructures and the derivation of the corresponding Fröhlich interaction. In Sec. II we describe the whole model in the particular case of a double heterostructure. The consequences of this phonon model for the Fröhlich electron-phonon coupling are reported. In Sec. III we examine the case of superlattices and in Sec. IV, single heterojunctions are considered.

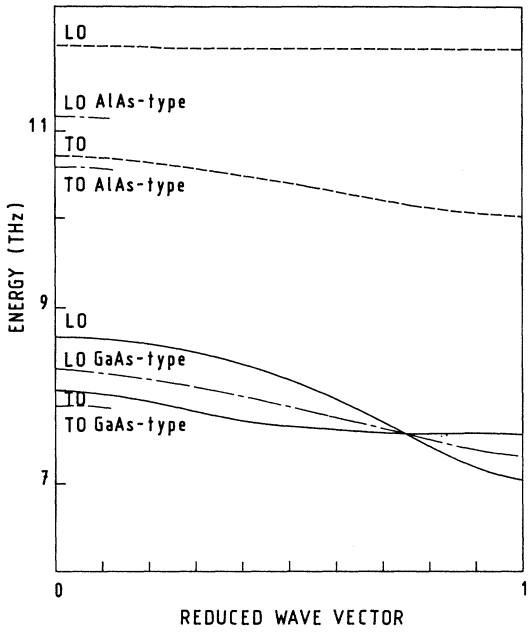

FIG. 1. Dispersion curves of the optical phonons in bulk GaAs (full line), in bulk AlAs (dashed line), in bulk $Al_{0.25}Ga_{0.75}As$ (dashed-dotted line) (Refs. 30 and 31).

II. POLARIZATION EIGENMODES OF A DOUBLE HETEROSTRUCTURE

The polar optical vibrations in simple ionic materials are important because of the polarization field associated with the ionic motion. As is well known, the charge transfer from the Ga atom to the As atom gives an ionic character to the GaAs crystal. The general expression for the atomic displacements associated with a normal mode in a three-dimensional crystal is given by

$$\mathbf{u}_{\alpha,j,q}(R_l)=(\hbar/2NVm_\alpha\omega_{j,q})^{1/2}\mathbf{e}_{\alpha,j,q} \times\exp(i\mathbf{q}\cdot\mathbf{R}_l-i\omega_{j,q}t)(b_{j,q}+b^\dagger_{j,-q})$$

where j refers to the mode (LO or TO), $\mathbf{q}$ is the wave vector, $\omega_{j,q}$ the eigenfrequency, α the atom (Ga or As) of atomic mass m_α, and $\mathbf{R}_l$ the position of the unit cell l. V is the volume of the crystal, N is the number of unit cells per unit of volume, and $\mathbf{e}_{\alpha,j,q}$ is the polarization eigenvector. $b_{j,q}$ and $b^\dagger_{j,-q}$ are the annihilation and creation operators. For optical modes, it has been found[32] that the most convenient parameter to choose for describing the optical type of motion is the displacement of the positive relative to the negative ions multiplied by the square root of their reduced mass:

$$\mathbf{w}_{j,q}(R_l)=(\hbar/2NV\omega_{j,q})^{1/2}\mathbf{e}_{j,q}\exp(i\mathbf{q}\cdot\mathbf{R}_l-i\omega_{j,q}t) \times(b_{j,q}+b^\dagger_{j,-q})$$

with

$$\mathbf{e}_{j,q}=(M/m_{\mathrm{Ga}})^{1/2}\mathbf{e}_{\mathrm{Ga},j,q}-(M/m_{\mathrm{As}})^{1/2}\mathbf{e}_{\mathrm{As},j,q}\ ,$$
$$\mathbf{e}^2_{\mathrm{Ga,j,q}}+\mathbf{e}^2_{\mathrm{As},j,q}=1\ ,$$
$$1/M=1/m_{\mathrm{Ga}}+1/m_{\mathrm{As}}\ .$$

Since for long-wavelength optical modes the center of mass of the unit cell does not move, we have also

$$(m_{\mathrm{Ga}})^{1/2}\mathbf{e}_{\mathrm{Ga},j,q}+(m_{\mathrm{As}})^{1/2}\mathbf{e}_{\mathrm{As},j,q}=\mathbf{0}\ ,$$

and it is easy to show that $|\mathbf{e}_{j,q}|=1$.

Therefore the LO polarization vector $\mathbf{e}_{j,q}$, which accounts for the displacements at the unit-cell scale, is a unit vector along the wave vector whatever the material is. This point enables us to focus on the study of the envelope wave function $\exp(i\mathbf{q}\cdot\mathbf{R})$. The formal transition of the microscopic theory to the continuum approach can be done by considering the limit of vanishing atomic distances under conservation of the material macroscopic dimensions. In that limit, we disregard displacements at the unit-cell scale. To establish the equation of motion for the atomic relative displacement envelope function, we go along the lines of the Born-Huang continuum theory.[32]

In the long-wavelength limit, the general form of the isotropic Lagrangian density for the atomic displacement field $\mathbf{w}$ is given by

$$\mathcal{L}=T-U=\tfrac{1}{2}\dot{\mathbf{w}}^2-\{\tfrac{1}{2}\gamma_1\mathbf{w}^2-\beta_a^2(\nabla\cdot\mathbf{w})^2-\beta_b^2[(\nabla w_x)^2+(\nabla w_y)^2+(\nabla w_z)^2]-\gamma_2\mathbf{w}\cdot\mathbf{E}-\gamma_3\mathbf{E}^2\}\ .$$

The first term is the kinetic energy. The three following terms account for the elastic energy due to the short-range forces and their explicit forms are dictated by symmetry considerations; the first one is the elastic energy of a collection of strings whereas the two following terms are due to the fact that these strings are not independent of each other and are the first terms to appear if the wave vector is nonzero. The next to last term is the dipole energy in an electric field and the last one is the electrostatic energy.

The momentum that is conjugate to w is

$$\pi=\delta\mathcal{L}/\delta\dot{\mathbf{w}}=\dot{\mathbf{w}}$$

and the Hamiltonian density is given by

$$\mathcal{H}=\tfrac{1}{2}\pi^2+\{\tfrac{1}{2}\gamma_1\mathbf{w}^2-\beta_a^2(\nabla\cdot\mathbf{w})^2-\beta_b^2[(\nabla w_x)^2+(\nabla w_y)^2+(\nabla w_z)^2]-\gamma_2\mathbf{w}\cdot\mathbf{E}-\gamma_3\mathbf{E}^2\}\ .$$

Then, the polarization field $\mathbf{P}$ is

$$\mathbf{P}=-\delta\mathcal{H}/\delta\mathbf{E}=\gamma_2\mathbf{w}+\gamma_3\mathbf{E}\ .$$

As is well known,[32] the γ coefficients can be expressed in terms of the measurable constants ω_{TO}, ϵ_s, ϵ_∞ which are, respectively, the TO-phonon frequency at zero wave vector, and the static and dynamic dielectric constants. The β coefficients are of the same order of magnitude as the velocity of the longitudinal acoustic mode of the material[23] and describe the optical modes dispersion curves in the Brillouin-zone center. The displacement field equation arises through the Euler-Lagrangian equation $d(\delta\mathcal{L}/\delta\dot{\mathbf{w}})/dt=\delta\mathcal{L}/\delta\mathbf{w}$:

$$\ddot{\mathbf{w}}(r,z)=-\omega_{\mathrm{TO}}^2\mathbf{w}(r,z)+(\epsilon_0\kappa_0-\epsilon_0\kappa_\infty)^{1/2}\omega_{\mathrm{TO}}\mathbf{E}-\beta_a^2\nabla(\nabla\cdot\mathbf{w})-\beta_b^2\Delta\mathbf{w} \tag{1}$$

with

$$\mathbf{P}=(\epsilon_0\kappa_0-\epsilon_0\kappa_\infty)^{1/2}\omega_{\mathrm{TO}}\mathbf{w}+(\epsilon_0\kappa_\infty-1)\mathbf{E}\ . \tag{2}$$

κ_0 and κ_∞ are the static and dynamic relative dielectric constants. κ_∞ accounts for the electronic polarizability of the ions and does not appear in a rigid-ion model. Finally, the electric field derives from the potential created by the polarization field (v is the unit-cell volume and the sum is performed over all the unit cells):[33]

$$\Phi(r,z)=\sum_l-\mathbf{P}(r_l,z_l)\cdot\nabla[1/(\mathbf{R}-\mathbf{R}_l)]/4\pi\epsilon_0=(1/v)\int d^2r'\int dz'\,\mathbf{P}(r',z')\cdot\nabla_{\mathbf{R}'}\times[1/(\mathbf{R}-\mathbf{R}')]/4\pi\epsilon_0\ ,$$
$$\mathbf{E}=-\nabla\Phi(r,z)\ . \tag{3}$$

Since the electric field derives from the potential created by the polarization field in the absence of any macroscopic density of charge, we have

$$\nabla\cdot\mathbf{D}=\nabla\cdot(\epsilon_0\mathbf{E}+\mathbf{P})=0\ .$$

In a bulk material,[23] the fields satisfying the above equations are either transverse fields with the dispersion relation

$$\omega^2=\omega_{\mathrm{TO}}^2-\beta_b^2k^2$$

or longitudinal fields with the dispersion relation

$$\omega^2=\omega_{\mathrm{LO}}^2-\beta^2k^2\ \text{ with }\beta^2=\beta_a^2+\beta_b^2\ .$$

We consider now a heterostructure composed of a thin layer of GaAs sandwiched between two much thicker layers of $\mathrm{Ga}_{1-x}\mathrm{Al}_x\mathrm{As}$. The z axis is perpendicular to the plane of the layers and the origin is taken in the middle of the GaAs layer of thickness L. We assume that the alloy behaves as an effective average crystal. This fictive ordered crystal has the alloy GaAs-like average lattice dynamics. Indeed, it has been recently shown that GaAs-like optical modes in the $\mathrm{Ga}_{1-x}\mathrm{Al}_x\mathrm{As}$ mixed crystal exhibit a well-defined downward dispersion curve.[30] Then, exploiting the translational invariance along the slab interfaces, we can look for an ionic displacement field such as

$$\mathbf{w}(r,z)=\xi(z)\exp(ikx)\exp(-i\omega t)\ ,$$

where the x axis has been taken along the in-plane wave vector. Because the coefficients entering into Eqs. (1)–(3), account for short-range forces or local properties of the materials, the displacement field obeys these equations in either material. The relative dielectric constants κ_0 and κ_∞ take into account the polarizability of the unit

cell either ionic or electronic. The transverse-optical frequency ω_{TO} is determined by the short-range force constant, the reduced mass, the effective charge of the ions, and their polarizability. The β coefficients should be determined by the ionic masses and the short-range force constants as the sound speed is.[24] Since the long-range Coulomb forces couple both materials, the electric field must be kept explicitly in the equation.

As we are looking for GaAs-like longitudinal-optical modes mainly localized in the GaAs slabs of heterostructures and as we suppose that they result of the hybridization of the LO waves of the different materials (Fig. 1), we look for irrotational displacements:

$$\nabla\times\mathbf{w}(r,z)=0 \text{ or } \xi_z(z)=\frac{1}{ik}\frac{d}{dz}\xi_x(z) .$$

Then, the atomic displacement field equations of motion become

$$\frac{d}{dz}\left[\beta^2\frac{d}{dz}\xi\right]+(\omega_{TO}^2-\omega^2-\beta^2k^2)\xi =(\epsilon_0\kappa_0-\epsilon_0\kappa_\infty)^{1/2}\omega_{TO}\mathbf{E} \quad (4)$$

with Eqs. (2) and (3).

In these equations, β^2, ω_{TO}, κ_0, and κ_∞ are step functions of z. $\beta^2 d^2/dz^2$ is written $(d/dz)(\beta^2 d/dz)$ in the same manner as the electronic eigenvalue equation in the effective-mass approximation should be written in the case of abrupt heterostructures.[34] Matching conditions are written by integrating the displacement field equation across the interfaces. Since the GaAs-$Ga_{1-x}Al_xAs$ heterostructures do not present microscopic interface modes,[24] we require that $\beta^2 d\xi(z)/dz$ should be continuous at the interfaces.

Eliminating the electric field between Eqs. (2) and (3), we get in each material:

$$\mathbf{w}=[(\epsilon_0\kappa_0-\epsilon_0\kappa_\infty)^{1/2}\omega_{TO}]^{-1} \times\left[\mathbf{P}+(\kappa_\infty-1)P_z\hat{\mathbf{z}} +\tfrac{1}{2}(\kappa_\infty-1)\int dz'\,k(\mathbf{P}\cdot\mathbf{K})\exp(-k|z-z'|)\mathbf{K}\right] \quad (5)$$

with

$$\mathbf{K}=\hat{\mathbf{x}}+i\,\mathrm{sgn}(z-z')\hat{\mathbf{z}} .$$

From $\nabla\times\mathbf{w}=\mathbf{0}$ and the above equation, we get $\nabla\times\mathbf{P}=\mathbf{0}$ and then $\nabla\times\mathbf{E}=\mathbf{0}$. All the fields are longitudinal and the Maxwell relations on the electric field and the electric displacement are fulfilled. From now on, we write

$$\mathbf{P}=\exp(i\mathbf{kr})[\varphi(z)\hat{\mathbf{x}}+(1/ik)(d\varphi/dz)\hat{\mathbf{z}}] .$$

Eliminating now w between Eqs. (1) and (5), we get an equation on φ:

$$\beta^2\kappa_\infty\, d^2\varphi/dz^2+(\omega_{TO}^2-\omega^2-\beta^2\kappa_\infty k^2)\varphi=\tfrac{1}{2}[\omega_{TO}^2(\kappa_0-1)+\omega^2(\kappa_\infty-1)]\int dz'\exp(-k|z-z'|)[k\varphi+\mathrm{sgn}(z-z')d\varphi/dz] .$$

Performing the integration in the right-hand side of the above equation gives

$$d^2\varphi/dz^2+\eta\varphi=-(\alpha/2)\{s_-\Sigma_-\exp[-s_-k(z+L/2)] +s_+\Sigma_+\exp[-s_+k(z-L/2)]\} \quad (6)$$

with

$$\alpha=[\omega^2(\kappa_\infty-1)-\omega_{TO}^2(\kappa_0-1)]/(\beta^2\kappa_\infty) ,$$
$$\eta=(\omega_{LO}^2-\omega^2)/\beta^2-k^2,\quad \omega_{LO}^2=\omega_{TO}^2\kappa_0/\kappa_\infty ,$$
$$s_-=\mathrm{sgn}(z+L/2) \text{ and } s_+=\mathrm{sgn}(z-L/2) ,$$
$$\Sigma_-=\varphi(-L/2_+)-\varphi(-L/2_-) ,$$
$$\Sigma_+=\varphi(L/2_+)-\varphi(L/2_-) .$$

This equation holds in each part of the heterostructure and the general solution is given by

$$\varphi= A\exp(iqz)+B\exp(-iqz) +\tfrac{1}{2}\langle[(1-1/\kappa_\infty)\omega^2-(1-1/\kappa_0)\omega_{LO}^2]/(\omega^2-\omega_{LO}^2)\rangle \times\{s_-\Sigma_-\exp[-s_-k(z+L/2)] +s_+\Sigma_+\exp[-s_+k(z-L/2)]\}$$

where q is a complex number verifying $q^2=\eta$.

We are interested in normal modes mainly localized near the GaAs quantum well. For that purpose, we look for phonons exponentially decreasing in the $Ga_{1-x}Al_xAs$ barriers ($\eta_{Ga\text{-}Al\text{-}As}<0$). The constants A and B are determined in each part of the heterostructure with that condition plus the continuity condition at the interfaces on $\beta^2 d\xi_x/dz$ and $\beta^2 d^2\xi_x/dz^2$. Finally, the normal modes are either even or odd function of z in a double heterostructure. All these conditions define an eigenequation on ω (see Appendix A). We do not find any pure interface modes with displacements exponentially decreasing from the interfaces. All solutions are found for $\eta_{GaAs}=(\omega_{GaAs,LO}^2-\omega^2)/\beta^2-k^2>0$. Each displacement field contains a sinusoidal part defining a confined mode behavior and an exponential part corresponding to an interface or Coulomb mode behavior. The interface mode behavior is associated with the macroscopic electric field oscillating in the whole heterostructure. Finally, to completely determine the displacement fields, we need a normalization condition. The general expression of the atomic displacements in a crystal periodic in two directions is given by

$$\mathbf{u}_{\alpha,j,k}(r_l,z_n)=(\hbar/2NSm_\alpha\omega_{j,k})^{1/2}\mathbf{e}_{\alpha,j,k}(z_n) \times\exp(i\mathbf{k}\cdot\mathbf{r}_l-i\omega_{j,k}t)(b_{j,k}+b_{j,-k}^\dagger)$$

where S is now the surface of the sample and N the number of unit cells per unit of surface. The other symbols have their usual meaning. The polarization eigenvector is normalized with

$$\sum_n \{[\mathbf{e}_{\mathrm{Ga},j,k}(z_n)]^2+[\mathbf{e}_{\mathrm{As},j,k}(z_n)]^2\}=1 .$$

Once again, we introduce the displacement of the positive relative to the negative ions multiplied by the square root of the reduced mass. For long-wavelength optical phonons, the normalization condition is now, if v is the unit-cell volume,

$$\sum_n [\mathbf{e}_{j,k}(z_n)]^2=1$$

or

$$\int dz[\mathbf{w}_{j,k}(r,z)]^2=v\hbar/(2S\omega_{j,k})$$

with

$$\mathbf{w}_{j,k}(r_l,z_n)=(\hbar/2NS\omega_{j,k})^{1/2}\mathbf{e}_{j,k}(z_n) \times\exp(i\mathbf{k}\cdot\mathbf{r}_l-i\omega_{j,k}t)(b_{j,k}+b^{\dagger}_{j,-k}) . \quad (7)$$

We define the symmetry of any mode by the symmetry of the z component of the corresponding displacement.

In Fig. 2, we present dispersion curves as functions of the in-plane wave vector for a 20-Å and a 150-Å GaAs-$Ga_{0.75}Al_{0.25}As$ quantum well.

In Fig. 3 the displacement envelope functions of the four higher modes are displayed for an in-plane wave vector of 10^6 cm^{-1}. The z components of the 150-Å quantum-well modes exhibit the features of well-confined modes with nodes at the interfaces except that the first mode which should behave like $\cos(\pi z/L)$ is absent for $k>10^5$ cm^{-1}. In agreement with microscopic theories, we do find a topmost cosinelike mode but it disappears as its dispersion curve reaches the GaAs one ($k\approx10^5$ cm^{-1}). Such a behavior cannot be tested against microscopic theories which are always applied to much thinner wells. On the contrary, this first even mode is found for all wave vectors in the 20-Å-wide quantum well. For this quantum-well width, the displacement fields spread out deeply in the barriers. However, the $k=0$ frequencies plotted on the GaAs-bulk dispersion curve correspond to $q=\pi/(m+0.5)a$ for the first mode and $q=2\pi/(m+1)a$ for the second mode. Therefore the displacements

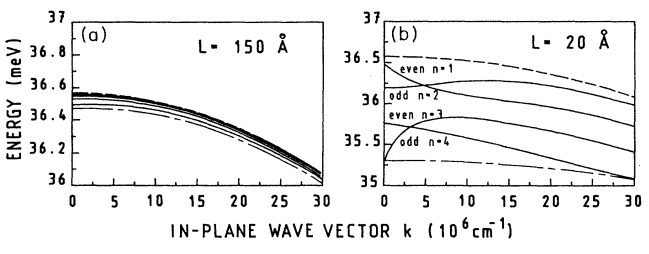

FIG. 2. Dispersion curves for the four higher-energy GaAs-like LO modes in two GaAs-$Ga_{0.75}Al_{0.25}As$ quantum wells with the LO dispersion curves in bulk GaAs (dashed line) and in bulk $Ga_{0.75}Al_{0.25}As$ (dashed-dotted line). The modes are labeled in decreasing energy order for a vanishing wave vector.

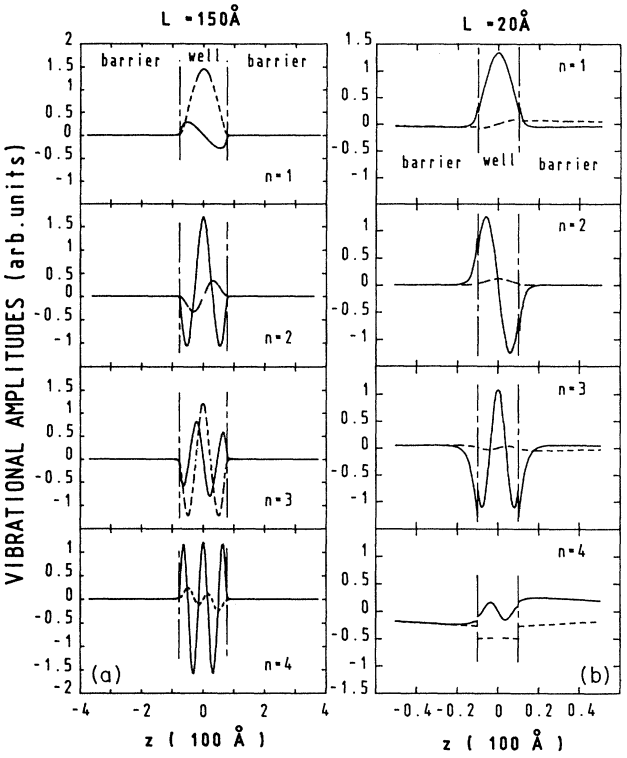

FIG. 3. Relative displacement envelope functions of the four higher-energy GaAs-like LO modes of two GaAs-$Ga_{0.75}Al_{0.25}As$ quantum wells for an in-plane wave vector $k=10^6$ cm^{-1}: full lines, z components; dashed lines, in-plane components. The modes are labeled in decreasing energy order for a vanishing wave vector disregarding the topmost cosinelike mode which disappears for $k>10^5$ cm^{-1}.

can extend deeply in the barriers for a nonzero in-plane wave vector even if the zone-center frequencies give roughly an extension of one monolayer. The in-plane components of the displacements have the inverse symmetry of the z components as it should be, but cannot be deduced simply by taking the sinusoidal function corresponding with the z component. This is obvious for the higher mode of a 150-Å quantum well where one should take in the well $u_x=1+\cos(2\pi z/L)$ rather than $u_x=\cos(2\pi z/L)$ or for the lower mode of the 20-Å quantum well where the sinusoidal part of the displacement appears only as a small modulation. A similar behavior has been reported in AlAs/GaAs superlattices[17] and is due to the exponential or "electrostatic" part of the displacements.

In Fig. 4 the envelope functions of the 20-Å well modes are displayed for an in-plane wave vector of 2×10^7 cm^{-1}. The modes are more localized in the well because their behavior in the barriers is mainly determined by the polarization field following an $\exp(-kz)$ decrease. Two modes display in their displacements an interface mode-like behavior. The first one is the $n=1$ even mode: the z component of its displacement field exhibits well-marked relative maxima at the interfaces for a 2×10^7 cm^{-1} in-plane wave vector. Besides, this displacement field along

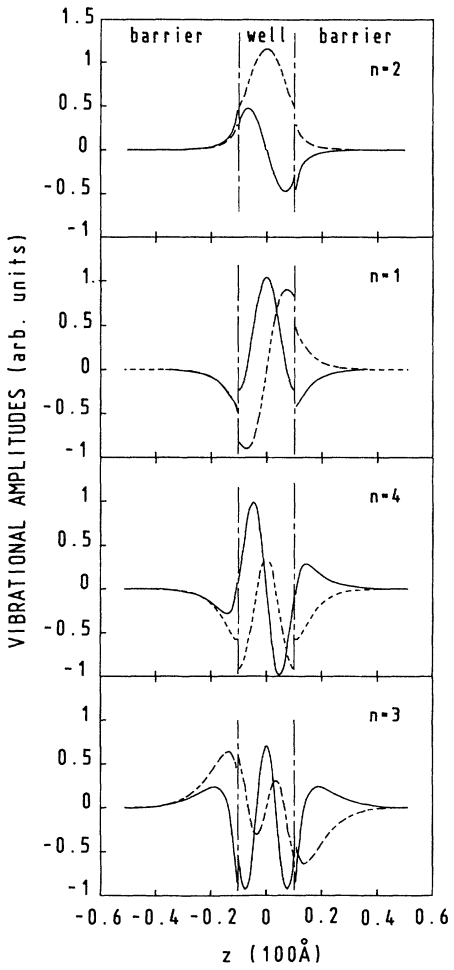

FIG. 4. Relative displacement envelope functions of the four higher-energy GaAs-like LO modes of 20-Å-wide GaAs-$Ga_{0.75}Al_{0.25}As$ quantum wells for an in-plane wave vector $k=2\times10^7$ cm^{-1}: full lines, z components; dashed lines, in-plane components. The modes are labeled in decreasing energy order for a vanishing wave vector.

the z axis bears a strong total dipole moment P within the quantum well because of its even parity and of its nonoscillating behavior. In the approximation of an infinitely thin well, this total dipole moment P induces the following electric field in the barriers:

$$\mathbf{E}(r,z)=[\exp(ikx)/2\epsilon_0][k\exp(-k|z|)]\times[P_z-i\,\mathrm{sgn}(z)P_x][\hat{\mathbf{z}}-i\,\mathrm{sgn}(z)\hat{\mathbf{x}}]\ . \quad (8)$$

Here P_x vanishes and P_z is roughly constant, being determined by the confined mode part of the displacement field. When k is nonzero, this electric field induces displacements in the barriers and therefore a relative decrease in the eigenfrequency of the mode. As the in-plane wave vector k goes to zero, the induced Coulomb field vanishes like k and the eigenfrequency strongly increases.

The $n=4$ odd mode displays an almost all interface modelike displacement feature: the x component of its displacement field exhibits well-marked absolute maxima at the interfaces for $k=2\times10^7$ cm^{-1}. Now P_z vanishes but P_x is no longer determined by the confined motion within the well. We believe that this normal mode is well described by the Fuchs-Kliewer odd interface mode:[21] it owes its existence to the presence of the interfaces of the double heterostructure and the displacement field is mainly determined by the matching of the dielectric constants of the materials through the interfaces. As the in-plane wave vector goes to zero, the induced Coulomb field spreads out in the barriers more deeply as $\exp(-k|z|)$ and the eigenfrequency strongly decreases.

We come now to the electron–optical-phonon interaction in quantum wells. The quantized interaction operator is straightforwardly derived from the displacement fields and the polarization fields through Eqs. (3) and (7). The general form of the resulting Hamiltonian is (see Appendices B and C):

$$H=\sum_k -ie(SL)^{-1/2}[\hbar\omega_{\mathrm{LO}}(1/\epsilon_\infty-1/\epsilon_0)/2]\times[\phi(z)/k]\exp(i\mathbf{k}\cdot\mathbf{r})(b_k+b^\dagger_{-k})$$

whereas for three-dimensional bulk phonons, the Hamiltonian may be written

$$H=\sum_{q,k} -ie(V)^{-1/2}[\hbar\omega_{\mathrm{LO}}(1/\epsilon_\infty-1/\epsilon_0)/2]\times[\exp(iqz)/(k^2+q^2)^{1/2}]\exp(i\mathbf{k}\cdot\mathbf{r})\times(b_{k,q}+b^\dagger_{-k,-q})\ .$$

In order to compare the interaction of quasi-two-dimensional electrons with bulk phonons or with quantized phonons, we have calculated the following coupling constants:

for quantized phonons ,

$$\alpha(k)=(1/L)\left|\int dz\,\zeta_i(z)\zeta_j(z)\phi_k(z)\right|^2 ,$$

and for bulk phonons,

$$\alpha(k)=(L_z/2\pi)\int dq[k^2/(k^2+q^2)]\times(1/L_z)\left|\int dz\,\zeta_i(z)\zeta_j(z)\exp(iqz)\right|^2$$

where $\zeta_i(z)$ is the electronic wave function of the i quantized level and L_z is the sample length in the z direction. We have considered intraband transitions within the first quantized electronic level ($i=j=0$) and interband transitions between the first and the second electronic quantized levels ($i=0$, $j=1$). For intraband transitions, only the first odd phonon mode has been considered and interband transitions have been calculated for the first even phonon mode. We have checked that for a quantum-well width lower than 250 Å, these phonons give roughly 90% of the total scattering rate: the higher mode functions $\phi(z)$ oscillate too much to match the electronic wave functions considered.

For a 50-Å quantum well and a 50-meV upper energy electronic state, the electron–LO-phonon scattering rate is roughly overestimated by a factor of 4 if the quantization of LO phonons is ignored (Fig. 5). The overestimation is even greater for lower quantum-well widths but

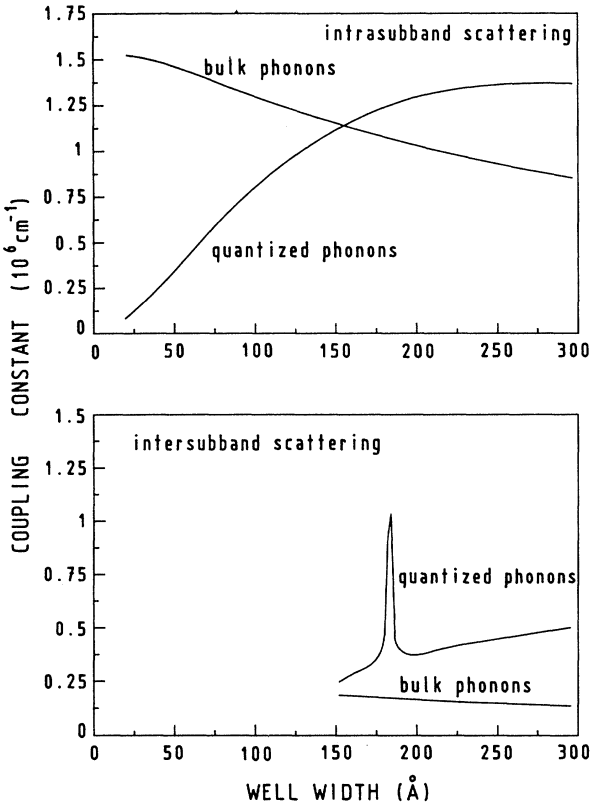

FIG. 5. Electron–LO-phonon scattering rate as a function of the GaAs-$Ga_{0.75}Al_{0.25}As$ quantum-well width. The involved electronic transition is between a 50-meV electronic state and a 14-meV electronic state. The initial and final electronic states have in-plane wave vectors in the same direction. These conditions give an in-plane phonon wave vector of 1.4×10^6 cm^{-1} for intrasubband scattering.

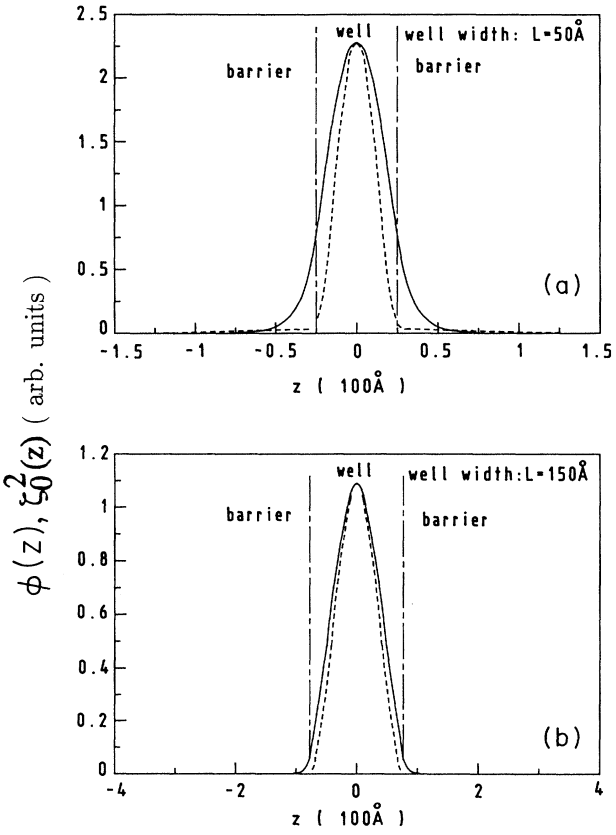

FIG. 6. Electronic probability function of the lowest quantum level (full line) and LO-phonon potential function (dashed line) for two GaAs-$Ga_{0.75}Al_{0.25}As$ quantum wells. The phonon mode is the higher-energy GaAs-like mode for a 1.4×10^6 cm^{-1} wave vector.

care should be taken because we have neglected the interaction with phonons propagating in the $Ga_{1-x}Al_xAs$ barriers and the electronic probability to be in the barriers begins to be large for those low well widths. This reduced scattering rate is fairly explained by the mismatch between the phonon function $\phi(z)$ and the electronic probability function $[\zeta_0(z)]^2$ which extends more deeply in the barriers (Fig. 6). As the well width increases, the electronic wave function becomes localized in the GaAs quantum well and fits the phonon envelope function $\phi(z)$: the quantized phonon scattering rate exceeds the bulk phonon scattering rate. The resonance in the interband scattering rate for a given electronic initial energy is due to the cancellation of the phonon wave vector when the intersubband electronic energy value is ω_{LO}. For very large quantum wells, one would expect that both scattering rates should be equal but the scattering rates for all wave vectors should be taken into account in a sum rule and a lot of quantized levels for both electrons and phonons should be involved.

As the upper electronic state energy increases, the in-plane wave vector k of the phonon interacting with the electrons decreases. However, the decrease of the in-plane wave vector k also implies an increase of the extension of the phonon wave function $\phi_k(z)$ in the barriers because of the Coulomb part of the phonon mode and, therefore, an increasing mismatch between the electronic density function and the phonon interaction function. This last effect dominates and, as is seen in Fig. 7, the bulk phonon scattering rate increases more quickly than the quantized phonon scattering rate when the upper electronic state energy increases.

Finally, we would like to emphasize that the lack of continuity of the displacement envelopes at the interfaces is due to the lack of continuity of the electrostatic field as expressed by the Maxwell relations. As the total energy of a mode is the sum of the kinetic energy of the atoms and of the electrostatic energy, the interaction potential, which we get from the integration of the polarization field [see (3)], is continuous across the interfaces.

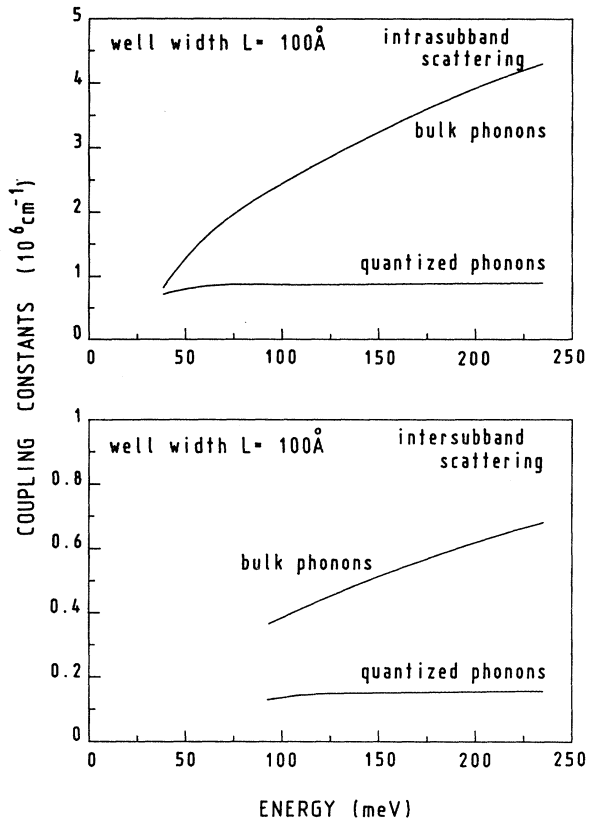

FIG. 7. Electron–LO-phonon scattering rate as a function of the upper electronic state energy. The initial and final electronic states have in-plane wave vectors in the same direction. The higher-energy odd phonon mode is considered for intrasubband scattering and the higher-energy even mode for intersubband scattering.

III. LONGITUDINAL-OPTICAL MODES IN SUPERLATTICES

The same formalism has been applied to $GaAs/Ga_{1-x}Al_xAs$ superlattices. Owing to the periodicity of the structure along the z axis, the general form of the envelope function of the displacement field and of the polarizability function is now

$$\mathbf{w}(r,z)=[\xi(z)\hat{\mathbf{x}}+(1/ik)(d\xi/dz)\hat{\mathbf{z}}]\exp(i\mathbf{k}\cdot\mathbf{r}) ,$$

$$\mathbf{P}(r,z)=[\varphi(z)\hat{\mathbf{x}}+(1/ik)(d\varphi/dz)\hat{\mathbf{z}}]\exp(i\mathbf{k}\cdot\mathbf{r})$$

with $\varphi(z)=f(z_0)e^{iQnd}$ and $\xi(z)=x(z_0)e^{iQnd}$,

$$z=z_0+nd, \quad 0<z_0<d .$$

d is the period of the superlattice and L is the GaAs well width. $f(z)$ and $x(z)$ are defined in the unit cell of the superlattice and the z component of the wave vector verifies:

$$-\pi/d<Q<\pi/d .$$

$\varphi(z)$ obeys the following equation if the origin is taken now on the left side of the well:

$$d^2\varphi/dz^2+\eta\varphi=(\alpha/2)[U\exp(-kz)+V\exp(kz)]$$

with

$$U=[e^{(k+iQ)L}\Sigma+f(0)-e^{(k+iQ)d}f(d)]/(1-e^{(k+iQ)d}) ,$$

$$V=-[e^{-(k-iQ)L}\Sigma+f(0)-e^{(k+iQ)d}f(d)]/(1-e^{(k+iQ)d}) ,$$

$$\Sigma=f(L_+)-f(L_i) .$$

The polarization is given in the first period by

$$\varphi=A\exp(iqz)+B\exp(-iqz)-\tfrac{1}{2}\langle[(1-1/\kappa_\infty)\omega^2-(1-1/\kappa_0)\omega_{LO}^2]/[\omega^2-\omega_{LO}^2]\rangle\times[U\exp(-kz)+V\exp(kz)] .$$

Expressing the boundary conditions at $z=L$ and at $z=d$ and the relations between φ and Σ, $f(0)$, $f(d)$ gives the eigenequation of the superlattice normal modes.

Contrary to the quantum-well case, the displacements in the barriers are made from the superposition of both real and imaginary argument exponentials; hence, barrier displacements are not necessarily expected to decay exponentially from the interfaces, particularly when the eigenfrequency approaches the $Ga_{1-x}Al_xAs$ dispersion curve.

Going from quantum wells to superlattices, we displayed in Fig. 8 the dispersion curves of 20-Å-wide well superlattices with infinite, 40-Å, and 20-Å barriers. Since the short-range force effects do not change with the barrier thickness for the modes mainly localized in the GaAs wells, we expect that only modes involving

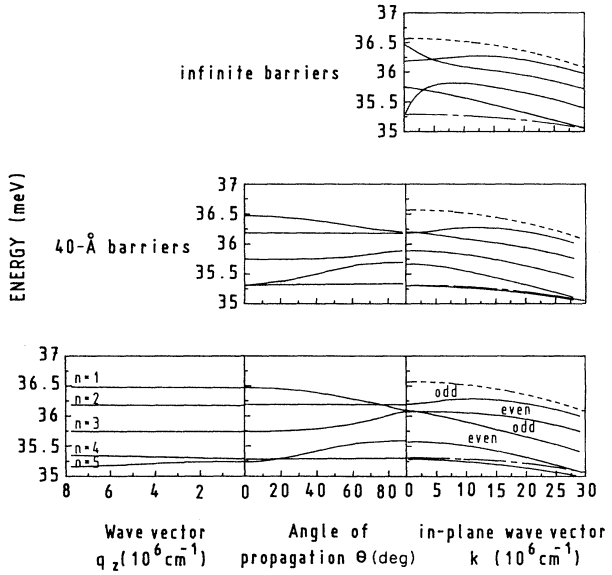

FIG. 8. Dispersion curves of GaAs-like LO phonons in three superlattices with 20-Å-wide GaAs slabs: infinite $Ga_{0.75}Al_{0.25}As$ barriers (top), 40-Å-wide $Ga_{0.75}Al_{0.25}As$ barriers (middle), 20-Å-wide $Ga_{0.75}Al_{0.25}As$ barriers (bottom). The eigenfrequencies are given for a wave vector along the superlattice axis (left-hand panel), for a vanishing wave vector, and as functions of the direction of propagation measured from the growth direction (central panel), for an in-plane wave vector (right-hand panel).

Coulomb fields will be affected by the decrease of the superlattice barriers. The energy dispersions as a function of the in-plane wave vector with a zero z component clearly exhibit the two Coulomb modes discussed previously for double heterostructures. To understand their behavior, we consider the dispersion curves as functions of the angle of propagation measured from the growth direction for a vanishing wave vector. These two Coulomb modes are the only ones showing an angular dispersion if we take into account the hybridization of modes of similar symmetry. Moreover, increasing the barrier thickness decreases the angular dispersion of these Coulomb modes. These facts strengthen the Coulomb origin of this angular dispersion, as has already been reported.[15,17]

To go further, we consider the displacements of the different modes (Fig. 9). For modes propagating along the z axis, the in-plane component of the displacements vanishes since we are dealing with longitudinal modes with no in-plane modulation. The displacements exhibit the features of confined modes. The modes with n odd are even modes whereas those with n even are odd ones. The Coulomb modes are labeled by $n=1$ and 5. This latter mode hybridizes with the $n=3$ mode because both of them are even. The total dipole moment within each slab is nonvanishing if n is odd and if the displacement envelope function does not strongly oscillate within the slab. Since the macroscopic electric field is determined by the total dipole moment in either slab, the Coulomb nature of the $n=1$ mode comes from the total dipole moment within the GaAs slabs whereas the $n=5$ mode has a strong dipole moment in the $Ga_{1-x}Al_xAs$ slabs (see left panel of Fig. 9). For a zero angle of propagation, this latter mode is a so-called $Ga_{1-x}Al_xAs$ quasiconfined mode,[13] as can also be inferred from the fact that its frequency falls below the edge of the overlap of the GaAs and $Ga_{1-x}Al_xAs$ continuum. Starting from modes propagating along the superlattice axis with well-confined displacement behavior and since we are dealing with modes with vanishing wave vectors, the induced Coulomb field behaves as the in-plane wave vector k [see Eq. (8)] and increases as the angle of propagation goes from 0 to $\pi/2$. The macroscopic Coulomb fields are effective when the in-plane wave-vector component is nonzero: for modes propagating along the growth direction, the frequencies are not affected by the barrier thickness (except for the $n=5$ quasiconfined mode). Since the Coulomb field will significantly spread out of the GaAs slab in the $Ga_{1-x}Al_xAs$ barrier, the $n=1$ mode frequency decreases with the angle of propagation of the mode relative to the z axis. On the contrary, the Coulomb field of the $n=5$ mode spreads out the $Ga_{1-x}Al_xAs$ slabs in the GaAs slabs so that its frequency increases with the angle of propagation.

Finally, we would like to point out that the parity of the $n=1$ mode changes as the angle of propagation goes from 0 to $\pi/2$. This behavior is allowed since the system does not bear any symmetry property for an arbitrary angle of propagation. However, this mode is the only one which displays a vanishing z component of its displacement field for an angle of $\pi/2$ whereas for most of the normal modes, the ratio of the displacement component along the superlattice axis on the in-plane displacement component is a function of the phase factor for the displacement field. Moreover, the real displacement fields do not have to be orthogonal to each other but the polarization eigenvectors verify this orthogonalization property.

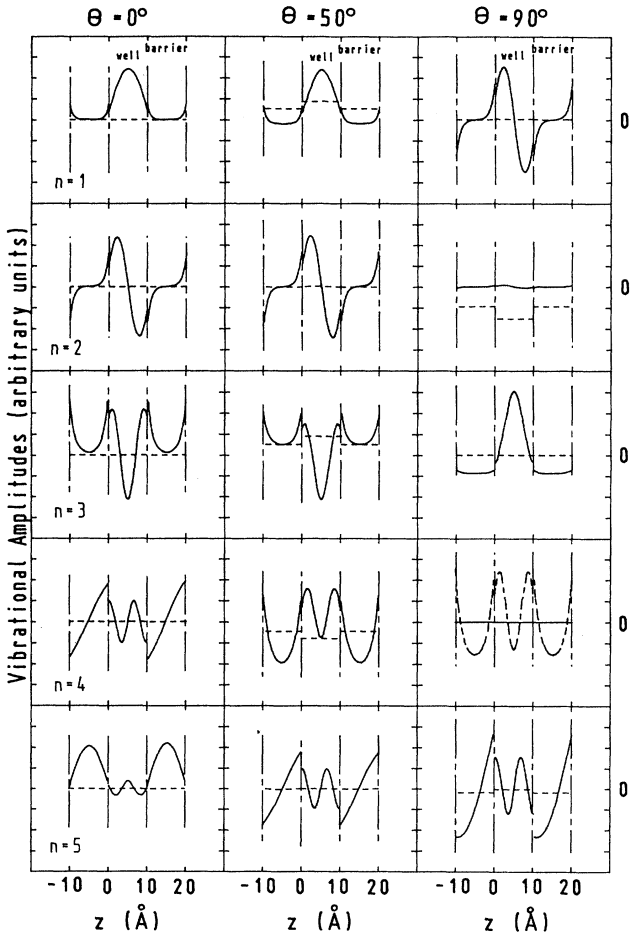

FIG. 9. Relative displacement envelope functions of the five higher-energy GaAs-like LO modes of a superlattice: GaAs wells and $Ga_{0.75}Al_{0.25}As$ barriers are 20 Å wide. In-plane components (full lines) and z components (dashed lines) of the displacements are given for a vanishing wave vector and three directions of propagation. From top to bottom, the modes are in decreasing energy order.

IV. LONGITUDINAL-OPTICAL MODES IN THE SINGLE HETEROJUNCTIONS

Calculations have been performed for single heterojunctions within the same formalism. The z component of the phonon wave vector is no longer quantized by a single heterojunction. Phonon normal modes are found for all energy values in the frequency range below the GaAs bulk frequency $(\omega^2_{LO,GaAs}-\beta^2_{GaAs}k^2)^{1/2}$ if k is the in-plane wave vector. For nonpropagative modes

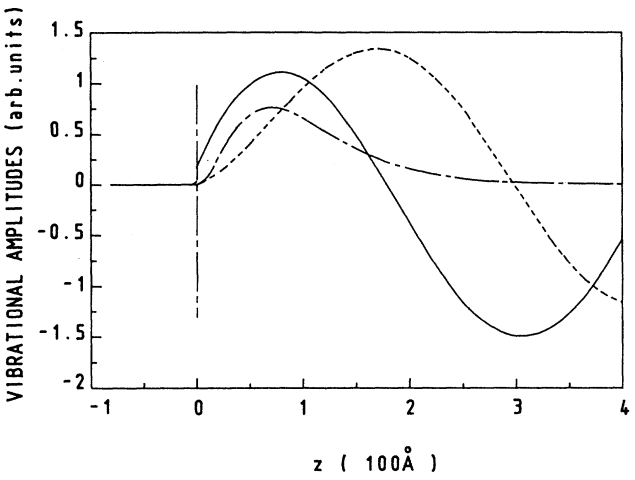

FIG. 10. Relative displacement envelope function of a GaAs-like LO phonon in a single GaAs/$Ga_{0.75}Al_{0.25}As$ heterojunction together with the electronic probability function of the first quantum level (dashed-dotted line): full line, z component; dashed line, in-plane component. The z component of the phonon wave vector is 1.3×10^6 cm^{-1}, the in-plane component is 10^6 cm^{-1}, and the electronic density is 3×10^{11}/cm^2.

$[\omega > (\omega^2_{LO,Ga-Al-As} - \beta^2_{Ga-Al-As}k^2)^{1/2}]$, the displacement field roughly undergoes a reflection on the GaAs/$Ga_{1-x}Al_xAs$ interface (Fig. 10). The general form of the electron–LO-phonon Hamiltonian is given by

$$H = \sum_{k,q} -ie(SL)^{-1/2}[\hbar\omega_{LO}(1/\epsilon_\infty - 1/\epsilon_0)/2] \times[\phi_{k,q}(z)/(k^2+q^2)^{1/2}]\exp(i\mathbf{k}\cdot\mathbf{r}) \times(b_{k,q}+b^\dagger_{-k,-q}) .$$

Taking into account only nonpropagative modes, we have calculated the following coupling constant in order to compare the scattering of electrons on bulk phonons and on heterojunction phonons:

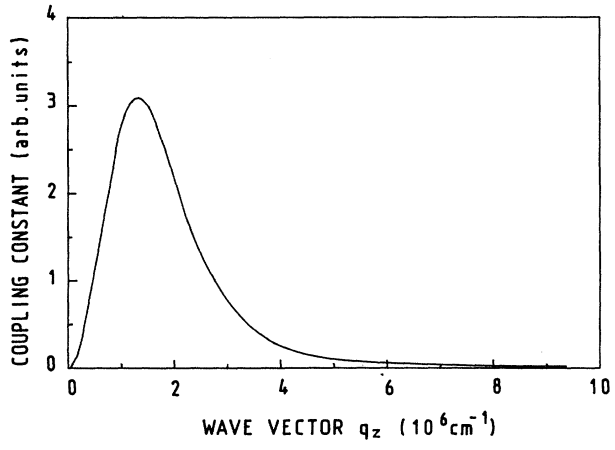

FIG. 11. Electron–LO-phonon intrasubband scattering rate as a function of the z component of the GaAs-like LO-phonon wave vector in a single GaAs-$Ga_{0.75}Al_{0.25}As$ heterojunction. The in-plane component is 10^6 cm^{-1} and the electronic density is 3×10^{11}/cm^2.

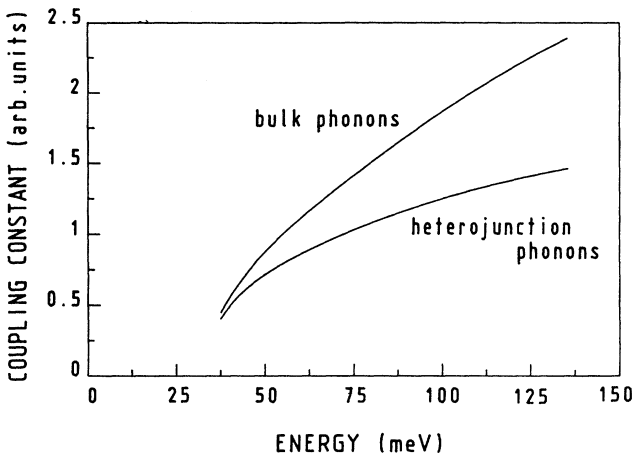

FIG. 12. Electron–LO-phonon intrasubband scattering rates as a function of the upper electronic state energy in a single GaAs-$Ga_{0.75}Al_{0.25}As$ heterojunction. The initial and final electronic states have in-plane wave vectors in the same direction.

for heterojunction phonons ,

$$\alpha(k) = (L_{GaAs}/2\pi)\int dq[k^2/(k^2+q^2)](1/L_{GaAs}) \times\left|\int dz[\zeta(z)]^2\phi_q(z)\right|^2 ,$$

and for bulk phonons,

$$\alpha(k) = (L_z/2\pi)\int dq[k^2/(k^2+q^2)] \times(1/L_z)\left|\int dz[\zeta(z)]^2\exp(iqz)\right|^2$$

where $\zeta(z)$ is the Fang-Howard electronic wave function and L_{GaAs} is the GaAs thickness. The electron-phonon scattering rate is peaked for the z component of the wave vector that gives the best fit between the electronic density and the phonon potential function along the growth axis (Figs. 10 and 11). Computing the scattering rates as functions of the upper electronic state energy, we recover the same behaviors as in quantum wells (Fig. 12).

V. CONCLUSION

In an attempt to establish an equivalent of the Fröhlich interaction in GaAs-$Ga_{1-x}Al_xAs$ heterojunctions ($x < 0.3$), we have investigated the nature of longitudinal-optical phonons in superlattices, quantum well, and single heterojunctions within a continuum approach. Assuming that the alloy behaves as an effective average crystal, the GaAs bulk LO band overlaps with the GaAs-like LO-phonon dispersion curve of the alloy. Therefore we have looked for normal modes as hybridizations of the corresponding bulk LO phonons. Boundary conditions have been derived by integrating the Euler-Lagrange equation of motion of the relative displacement field provided that this one is written in a Hermitian

form. We do not find any pure interface mode but every normal mode contains a Coulomb displacement field besides a confined motion. Two kinds of Coulomb modes come out: either the total dipole moment within a slab is nonzero and induces an electric field within the other slab or the presence of interfaces allows the emergence of a Fuchs-Kliewer mode through the matching of the dielectric functions. The long-range Coulomb interaction shows up in the dispersion curves as a function of the in-plane wave vector for superlattices with decreasing barrier thicknesses because the short-range forces involved in modes mainly localized in the GaAs slabs are not affected by the $Ga_{1-x}Al_xAs$ thickness. Finally, the electron-phonon interaction is strongly reduced in quantum wells for well widths lower than 100 Å. This reduction is attributed to the mismatching between the quantized phonon potential function in the z direction and the electronic density function which spreads out more deeply in the barriers.

APPENDIX A: EIGENEQUATION FOR A DOUBLE HETEROSTRUCTURE

We give the coefficients of the 3×3 matrix defining the eigenfrequencies ω. All quantities related to the GaAs quantum well are labeled by w whereas those concerning the $Ga_{1-x}Al_xAs$ barriers are labeled by b:

$$q_w=(\omega_{w,\mathrm{LO}}^2-\omega^2-\beta_w^2k^2)^{1/2}/\beta_w ,$$

$$q_b=(\omega^2-\beta_{b,\mathrm{LO}}^2+\beta_b^2k^2)^{1/2}/\beta_b ,$$

$$\Delta=[(1-1/\kappa_\infty)\omega^2-(1-1/\kappa_0)\omega_{\mathrm{LO}}^2]/(\omega^2-\omega_{\mathrm{LO}}^2) ,$$

$$X=\Delta-1+1/\kappa_\infty ,$$

$$R=[(\kappa_{0w}-\kappa_{\infty w})^{1/2}\omega_{w,\mathrm{TO}}/\kappa_{\infty w}]/[(\kappa_{0b}-\kappa_{\infty b})^{1/2}\omega_{b,\mathrm{TO}}/\kappa_{\infty b}] ,$$

$$C=-\frac{(\beta_w^2q_w^2+P\beta_b^2q_b^2)\cos(q_wL/2)}{P\beta_b^2q_b^2+\exp(-kL/2)[\cosh(kL/2)(\beta_w^2k^2X_w-\Delta_wR\beta_b^2q_b^2)+R\sinh(kL/2)(\beta_b^2k^2X_b-\Delta_b\beta_b^2q_b^2)]} .$$

Odd modes:

$$a_{11}=\cos(q_wL/2) ,$$

$$a_{12}=-1 ,$$

$$a_{13}=1-\exp(-kL/2)[\Delta_w\cosh(kL/2)+\Delta_b\sinh(kL/2)] ,$$

$$a_{21}=\beta_w^2q_w\sin(q_wL/2) ,$$

$$a_{22}=-R\beta_b^2q_b ,$$

$$a_{23}=k\exp(-kL/2)\sinh(kL/2)(\beta_w^2X_\omega-R\beta_b^2X_\beta) ,$$

$$a_{31}=\beta_w^2q_w^2\cos(q_wL/2) ,$$

$$a_{32}=R\beta_b^2q_b^2 ,$$

$$a_{33}=k^2\exp(-kL/2)[\beta_w^2X_\omega\cosh(kL/2)+P\beta_b^2X_b\sinh(kL/2)] .$$

Even modes:

$$a_{11}=\sinh(q_wL/2) ,$$

$$a_{12}=-1 ,$$

$$a_{13}=1-\exp(-kL/2)[\Delta_w\sinh(kL/2)+\Delta_b\cosh(kL/2)] ,$$

$$a_{21}=\beta_w^2q_w\cos(q_wL/2) .$$

$$a_{22}=R\beta_b^2q_b ,$$

$$a_{23}=k\exp(-kL/2)\cosh(kL/2)(P\beta_b^2-X_\beta\beta_w^2X_\omega) ,$$

$$a_{31}=\beta_w^2q_w^2\sin(q_wL/2) ,$$

$$a_{32}=R\beta_b^2q_b^2 ,$$

$$a_{33}=k^2\exp(-kL/2)[\beta_w^2X_\omega\sinh(kL/2)+P\beta_b^2X_b\cosh(kL/2)] .$$

APPENDIX B: ATOMIC DISPLACEMENTS

Odd modes:

$$C=\frac{-[\beta_w^2 q_w^2+R\beta_b^2 q_b^2]\cos(q_w L/2)}{R\beta_b^2 q_b^2+\exp(-kL/2)[\cosh(kL/2)(\beta_w^2 k^2 X_w-\Delta_w R\beta_b^2 q_b^2)+R\sinh(kL/2)(\beta_b^2 k^2 X_b-\Delta_b\beta_b^2 q_b^2)]},$$

$$B=\cos(q_w L/2)+C\{1-\exp(-kL/2)[\Delta_w\cosh(q_w L/2)+\Delta_b\sinh(q_b L/2)]\},$$

$$A^2=(L/2)/\left[\int_0^{L/2}dz\,(u_x^2+u_z^2)+\int_{L/2}^{\infty}dz\,(u_x^2+u_z^2)\right],$$

$$U_x=Au_x,$$

$$U_z=Au_z.$$

$|z|<L/2$:

$$u_x=\{\kappa_{\infty w}/[(\epsilon_{0w}-\epsilon_{\infty w})^{1/2}\omega_{w,\mathrm{TO}}]\}[\cos(q_w z)-X_w C\exp(-kL/2)\cosh(kz)],$$

$$iu_z=\{\kappa_{\infty w}/[(\epsilon_{0w}-\epsilon_{\infty w})^{1/2}\omega_{w,\mathrm{TO}}]\}[-(q_w/k)\sin(q_w z)-X_w C\exp(-kL/2)\sinh(kz)].$$

$z>L/2$:

$$u_x=\{\kappa_{\infty b}/[(\epsilon_{0b}-\epsilon_{\infty b})^{1/2}\omega_{b,\mathrm{TO}}]\}\{B\exp[-q_b(z-L/2)]+X_b\sinh(kL/2)C\exp(-kz)\},$$

$$iu_z=\{\kappa_{\infty b}/[(\epsilon_{0b}-\epsilon_{\infty b})^{1/2}\omega_{b,\mathrm{TO}}]\}\{-(q_b/k)B\exp[-q_b(z-L/2)]-X_b\sinh(kL/2)C\exp(-k,z)\}.$$

Even modes:

$$C=\frac{-[\beta_w^2 q_w^2+P\beta_b^2 q_b^2]\sin(q_w L/2)}{P\beta_b^2 q_b^2+\exp(-kL/2)}[\sinh(kL/2)(\beta_w^2 k^2 X_w-\Delta_w R\beta_b^2)+R\cosh(kL/2)(\beta_b^2 k^2 X_b-\Delta_b\beta_b^2 q_b^2)],$$

$$B=\sin(q_w L/2)+C\{1-\exp(-kL/2)[\Delta_w\sinh(q_w L/2)+\Delta_b\cosh(q_b L/2)]\},$$

$$A^2=(L/2)\left[\int_0^{L/2}dz(u_x^2+u_z^2)+\int_{L/2}^{\infty}dz(u_x^2+u_z^2)\right],$$

$$U_x=Au_x,$$

$$U_z=Au_z.$$

$|z|<L/2$:

$$u_x=\{\kappa_{\infty w}/[(\epsilon_{0w}-\epsilon_{\infty w})^{1/2}\omega_{w,\mathrm{TO}}]\}[\sin(q_w z)-X_w C\exp(-kL/2)\sinh(kz)],$$

$$iu_z=\{\kappa_{\infty w}/[(\epsilon_{0w}-\epsilon_{\infty w})^{1/2}\omega_{w,\mathrm{TO}}]\}[(q_w/k)\cos(q_w z)-X_w C\exp(-kL/2)\cosh(kz)].$$

$z>L/2$:

$$u_x=\{\kappa_{\infty b}/[(\epsilon_{0b}-\epsilon_{\infty b})^{1/2}\omega_{b,\mathrm{TO}}]\}\{B\exp[-q_b(z-L/2)]+X_b\cosh(kL/2)C\exp(-kz)\},$$

$$iu_z=\{\kappa_{\infty b}/[(\epsilon_{0b}-\epsilon_{\infty b})^{1/2}\omega_{b,\mathrm{TO}}]\}\{-(q_b/k)B\exp[-q_b(z-L/2)]-X_b\cosh(kL/2)C\exp(-kz)\}.$$

APPENDIX C: ELECTRON-PHONON INTERACTION

We give the electron-phonon interaction potential in double heterostructures.
Odd modes:

$$H=ieA(SL)^{-1/2}[h\omega_{\mathrm{LO}}(1/\epsilon_\infty-1/\epsilon_0)/2]\exp(ikr)(b_k+b^{\dagger}_{-k})(1/k)xT.$$

$z<-L/2$:

$$T=RB\exp[q_b(z+\tfrac{1}{2})]+RC(\Delta_b-1)\sinh(kL/2)\exp(kz),$$

$|z|<L/2$:

$$T=\cos(q_w z)+C(1-\Delta_w)\exp(-kL/2)\cosh(kz).$$

$z>L/2$:

$$T=RB\exp[-q_b(z-\tfrac{1}{2})]+RC(\Delta_b-1)\sinh(kL/2)\exp(-kz).$$

Even modes:

$$H=-ieA(SL)^{-1/2}[\hbar\omega_{\mathrm{LO}}(1/\epsilon_\infty-1/\epsilon_0)/2]\exp(ikr)(b_k+b^\dagger_{-k})(1/k)xT \ .$$

$z<-L/2$:

$$T=-RB\exp[q_b(z+\tfrac{1}{2})]-RC(\Delta_b-1)\cosh(kL/2)\exp(kz) \ .$$

$|z|<L/2$:

$$T=\sin(q_w z)+C(1-\Delta_w)\exp(-kL/2)\sinh(kz) \ .$$

$z>L/2$:

$$T=RB\exp[-q_b(z-\tfrac{1}{2})]+RC(\Delta_b-1)\cosh(kL/2)\exp(kz) \ .$$

[1]B. Jusserand, D. Paquet, and A. Regreny, Phys. Rev. B **30**, 6245 (1984).

[2]C. Colvard, T. A. Gant, M. V. Klein, R. Merlin, R. Fischer, H. Morkoç, and A. C. Gossard, Phys. Rev. B **31**, 2080 (1985).

[3]A. K. Sood, J. Menendez, M. Cardona, and K. Ploog, Phys. Rev. Lett. **54**, 2111 (1985); **54**, 2115 (1985).

[4]M. Nakayama, K. Kubota, H. Kato, and N. Sano, J. Appl. Phys. **60**, 3289 (1986).

[5]G. Fasol, M. Tanaka, H. Sakaki, and Y. Horikoshi, Phys. Rev. B **38**, 6056 (1988).

[6]Z. P. Wang, H. X. Han, G. H. Li, D. S. Jiang, and K. Ploog, Phys. Rev. B **38**, 8483 (1988).

[7]B. Jusserand and D. Paquet, Phys. Rev. Lett. **56**, 1752 (1986).

[8]H. Chu, S. F. Ren, and Y. C. Chang, Phys. Rev. B **37**, 10 746 (1988).

[9]E. Molinari, A. Fasolino, and K. Kunc, Phys. Rev. Lett. **56**, 1751 (1986).

[10]J. E. Zucker, A. Pinczuk, D. S. Chemla, A. C. Gossard, and W. Wiegmann, Phys. Rev. Lett. **53**, 1280 (1984).

[11]A. S. Barker, J. L. Merz, and A. C. Gossard, Phys. Rev. B **17**, 3181 (1978).

[12]A. Fasolino, E. Molinari, and J. C. Maan, Phys. Rev. B **33**, 8889 (1986).

[13]A. Fasolino, E. Molinari, and J. C. Maan, Phys. Rev. B **39**, 3923 (1989).

[14]E. Richter and D. Strauch, Solid State Commun. **64**, 867 (1987).

[15]S. F. Ren, H. Chu, and Y. C. Chang, Phys. Rev. Lett. **59**, 1841 (1987); Phys. Rev. B **37**, 8899 (1988).

[16]T. Tsuchiya, H. Akera, and T. Ando, Phys. Rev. B **39**, 6025 (1989).

[17]K. Huang and B. F. Zhu, Phys. Rev. B **38**, 2183 (1988); **38**, 13 377 (1988).

[18]B. F. Zhu, Phys. Rev. B **38**, 7694 (1988).

[19]E. P. Pokatilov and S. I. Beril, Phys. Status Solidi B **110**, K75 (1982); **118**, 567 (1983).

[20]L. Wendler, Phys. Status Solidi B **129**, 513 (1985).

[21]R. Fuchs and K. L. Kliewer, Phys. Rev. **140**, A2076 (1965).

[22]F. Bechstedt and H. Gerecke, Phys. Status Solidi B **156**, 151 (1989).

[23]M. Babiker, J. Phys. C **19**, 683 (1986).

[24]H. Akera and T. Ando, Phys. Rev. B **40**, 2914 (1989).

[25]N. Mori and T. Ando, Phys. Rev. B **40**, 6175 (1989).

[26]J. Shah, A. Pinczuk, A. C. Gossard, and W. Wiegmann, Phys. Rev. Lett. **54**, 2045 (1985).

[27]C. H. Yang, J. M. Carlson-Swindle, S. A. Lyon, and J. M. Worlock, Phys. Rev. Lett. **55**, 2359 (1985).

[28]N. Balkan, B. K. Ridley, M. Emeny, and I. Goodridge, Semicond. Sci. Technol. **4**, 852 (1989).

[29]C. Guillemot, F. Clérot, P. Auvray, M. Baudet, M. Gauneau, and A. Regreny, Superlatt. Microstruct. **8**, 259 (1990).

[30]B. Jusserand, D. Paquet, and F. Mollot, Phys. Rev. Lett. **63**, 2397 (1989).

[31]S. Adachi, J. Appl. Phys. **58**, R1 (1985).

[32]M. Born and K. Huang, *Dynamical Theory of Crystal Lattices* (Oxford University Press, Oxford, 1954).

[33]H. Haken, *Quantum Field Theory Of Solids* (North-Holland, Amsterdam, 1976).

[34]G. T. Einevoll, P. C. Hemmer, and J. Thomsen, Phys. Rev. B **42**, 3485 (1990).